

Active Nematics at Bifurcations

Zhengyang Liu,¹ Claire Doré,¹ Antonio Tavera-Vazquez,^{1,2} and Teresa Lopez-Leon¹

¹*Laboratoire Gulliver, UMR 7083 CNRS, ESPCI Paris, PSL Research University, 75005 Paris, France.*

²*Pritzker School of Molecular Engineering, University of Chicago, Chicago, IL 60637, USA.*

(Dated: October 14, 2024)

Under lateral confinement, active matter self-organize into coherent flows. Such behavior implies the possibility of achieving logical operations in properly designed channel networks. Bifurcations are a key ingredient in channel networks. Understanding active matter behavior at bifurcations is therefore an important step towards a proper channel network design. In this paper, we experimentally explore active matter behavior at bifurcations using the microtubule-kinesin model system. Specifically, we compare the effects of channel length, ratchets and turning angles. Our results suggest that ratchets and turning angles help establish unambiguous polarized flow states. In contrast, channel length is a less relevant factor, which results in more frequently changing flow states. Our experiment is the first step to understanding active nematic flows in complex channel networks. The result lays the foundation for active matter logic and computation.

I. INTRODUCTION

Active matter flows spontaneously under channel confinement, forming coherent flows [1–5]. Such behavior implies several possible applications of active matter, including serving as micro-scale transport, soft robotics and active matter logic [6, 7]. Boundary-mediated control has been shown effective in manipulating active matter in both experiments [1–4, 8–10] and simulations [11–14]. As of now, most studies have focused on the behavior of active matter in stand-alone smooth channels, which showed that active flows were intrinsically bistable [2, 3]. However, to realize the full potential of active matter channel flows, it is necessary to study the behavior of active matter in channel networks and with asymmetric geometries, as suggested in the pioneering active matter logic work by Woodhouse and Dunkel [7]. Very recently, channel networks attract more attention, and frustrated flow states have been investigated in coupled annular rings [5] and large honeycomb-like networks [15]. The other essential component of active matter logic is the diode channel, which only permits flow in one direction. While a few early works have hinted or employed asymmetric geometries, such as a kink or an array of ratchet teeth, to steer active matter flows [2, 5, 14, 16–18], a systematic study of asymmetric channels in the context of channel networks is still missing.

In this work, we filled this gap by experimentally studying the flow behavior of active matter at channel networks consisting of asymmetric channels. To obtain a clear understanding, we studied the simplest possible form of a channel network – the bifurcation – where a channel splits into two at a node. Despite of being simple, the bifurcation is a key element of more complex channel networks, and a great system to study frustrated flow states. Assymetry are in two levels: in single channel level, ratchets are introduced to favor the flow in a certain direction; in network level, input channels are designed to split into channels with different lengths, number of ratchets and turning angles. Our results suggest

that ratchets and turning angles help establish stable polarized flow states, where the inlet flow primarily goes into one of the outlet channels, leaving the other channel with little flow. In contrast, channel length is a less relevant factor, which results in more frequently changing flow states. **Topological defects show different dynamics are different in flowing ratchet channels from frustrated straight channels, uncovering the steering mechanism of the ratchets.** Our experiment is the first step to understanding active nematic flows in complex channel networks. The result lays the foundation for potential applications of active flow networks in mass transport and flow computation.

II. EXPERIMENT

Our active matter system comprises microtubule filaments powered by ATP-consuming two-headed kinesin molecular motors [19]. By adding depleting agent poly (ethylene glycol) (PEG), the system forms dense bundles at the water-oil interface. Driven by the kinesin motors, the bundles stretch and bend constantly, exhibiting chaotic flows characterized by the formation and annihilation of topological defects. In an experiment, 2.5 μL of microtubule solution was put in a custom pool of 5 mm diameter, covered by 100 μL of silicone oil (5 cSt). The micro-printed bifurcation channel structure was then gently placed at the oil-water interface, confining the chaotic system into channel flows (Fig. 1(a)). An unconfined active nematics system is shown in Fig. 1(b), while the same system confined by the bifurcation channels is shown in Fig. 1(c). The active nematics system is observed using a confocal microscope (Nikon), and images are taken at 2 Hz using a 10X objective lens. Then, 400 μm of each channel is cropped and analyzed by PIV, as shown in Fig. 2(a).

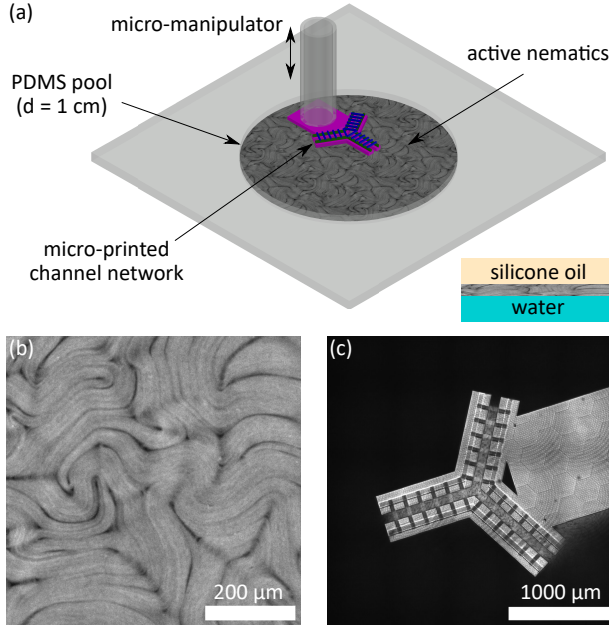


FIG. 1. Confining microtubule-kinesin system at water-oil interface – the experimental setup. (a) Schematic diagram of the experimental setup. The microtubule-kinesin active nematic system is placed at an water-oil interface in a custom PDMS pool, and is subject to lateral confinement by the micro-printed bifurcation channel. (b) Confocal image of a mature interfacial microtubule-kinesin system. (c) Confocal image of the bifurcation channels set on the interfacial microtubule-kinesin system.

III. RESULTS

A. Symmetric bifurcation

We first studied the flow behavior at a symmetric bifurcation, where all the channels are smooth and of the same length. To extract the flow rate in each channel, we cropped regions 400 μm from the connecting node for each channel and performed Particle Image Velocimetry (PIV) analysis (as indicated by the rectangles in Fig. 2(a)). Snapshots of the PIV results are shown in Fig. 2(b). Local velocity vectors $v(x, y)$ are indicated as yellow arrows, where x and y are defined separately as the transverse and parallel directions for each channel, respectively.

The surface flow rate in the channel direction (Q_y) was calculated by integrating the velocity field over the channel cross-section. To minimize the noise in data, we also average the flow rate calculated at different y positions. Formally, our channel flow rate is defined as

$$\phi = \langle Q_y \rangle = \frac{1}{L} \int_0^L Q_y dy, \quad (1)$$

where $Q_y = \int_{x_1}^{x_2} v_y(x, y) dx$ is the flow rate at y position, L is the length of the cropped image, and x_1 and x_2 are the left and right boundaries of the channel, respectively.

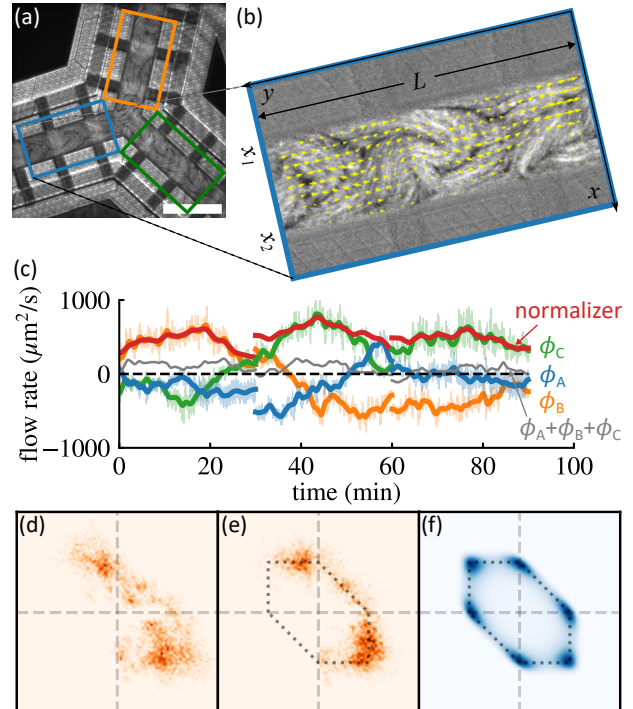


FIG. 2. Flow rate measurements and flow rate histogram. (a) A snapshot of microtubule-kinesin system confined in bifurcation channels. The scale bar is 200 μm. The rectangles indicate the regions where PIV analysis was performed. (b) Zoom-in view of channel A, yellow arrows indicates local velocity from PIV analysis. (c) Flow rate time series in the 3 channels A (blue), B (orange) and C (green). The light curves in the back are the real flow rates, while the bold curves in the front are Gaussian-smoothed flow rates with $\sigma = 25$ s. The “normalizer” and the sum of all flow rates are shown as red and gray, respectively. (d) Raw, (e) normalized and (f) theoretical flow rate histogram of channel B and C.

For consistency, we always define positive flow rate as the flow away from the connecting node. With this definition, the mass conservation at the connecting node can be expressed as $\phi_A + \phi_B + \phi_C = 0$.

The flow rates in channels A, B and C over time are plotted in Fig. 2(c) in blue, orange and green curves, respectively, corresponding to the colors of the rectangles in Fig. 2(a). The light curves in the back are the real flow rates, while the bold curves in the front are Gaussian-smoothed flow rates with $\sigma = 25$ s. The gray curve is the sum of the flow rates in the 3 channels, $\phi_A + \phi_B + \phi_C$, which serves as a check for mass conservation. The magnitude of the gray curve is much smaller than the flow rates in the 3 channels, indicating that mass conservation is indeed satisfied at the connecting node. Figures 2(d) show the histograms of raw flow rates in channels B and C. Darker colors indicate higher probability of flow rate configurations, and the crossing points of the dashed lines are the origin of the histogram ($\phi_B = \phi_C = 0$). We only show the histogram of the

flow rates in channels B and C, because the flow rates are constrained by $\phi_A + \phi_B + \phi_C = 0$, meaning that two flow rates are enough to specify the flow configuration. Since we were interested in the flow configurations, that is, how a flow in one channel was distributed in the other two channels, we focused on the normalized flow rates $\tilde{\phi}_A$, $\tilde{\phi}_B$ and $\tilde{\phi}_C$. This eliminated the effect of the fluctuating overall flow rates (for detailed normalization procedure, see Supplemental Information). The normalized flow rate histograms are shown in Fig. 2(e). Flow configurations that conserve mass is indicated by elliptic hexagons in dotted lines. The normalized flow rate histogram show good agreement with the mass conservation line, which is reassuring for our experimental and analytical techniques. It is possible to obtain the theoretical flow rate histogram by solving the Landau-type model proposed by Woodhouse and Dunkel [7]. In short, the model states that the flow in a channel network tends to minimize the total energy of the system, which comprises channel flow energy, diode energy and mass conservation energy. Formally, the Hamiltonian of the system to be minimized is

$$H = H_{\text{channel}} + H_{\text{diode}} + H_{\text{mass}}, \quad (2)$$

the detailed form of the Hamiltonian can be found in the original paper [7] and Supplemental Information. By simulating the flow configurations in a Monte Carlo process, we obtained a theoretical flow rate histogram, as shown in Fig. 2(f). Compared to the theoretical flow rate histogram in Fig. 2(f), the experimental histogram shows a broader distribution, covering most of the possible configurations of flow rates in the 3 channels. Sharp peaks at polarized flow configurations, where one of the channels is a completely frustrated, however, were not observed in our experiment. It is worth noting that although the channels were designed to be fully symmetric, the grid requires a base structure to which the micromanipulator is attached (see Fig. 1(c)), which may result in asymmetry in the flow rates. This is probably the reason why we did not observe all the flow configurations that satisfy mass conservation, especially those where $\tilde{\phi}_A = 1$.

B. Assymetry in channel length

To test the

Having learned from the fully symmetric bifurcation experiment, we enforce channel A as a ratchet channel, which guarantees that $\phi_A < 0$. We then study the effect of channel length on the flow behavior. In Fig.3(a), we show the flow behavior at a 9-teeth ratchet inlet with

2 equal length outlets. The flow fluctuates between polarized and non-polarized states, exploring all the possible configurations. The equal splitting state is the most probable configuration. It is also noticed that channels B and C are always outlets when fixing A as the inlet with ratchets. This observation implies that the ratchet channel has a dominant effect on the flow behavior, compared to the straight channels. Such dominance will be further confirmed in the following experiments. In Fig.3(b), we show the flow behavior at a 4-teeth ratchet inlet with long and short outlets. The expectation from theory is that the flow will prefer the longer outlet, as the longer path has a lower energy state and is therefore more energetically favorable. However, we observe that the flow explores all the possible configurations, showing no preferred splitting ratio. In Fig.3(c), we show the flow behavior at a 4-teeth ratchet inlet with 2 equal length outlets. This experiment is done to keep consistent ratchet numbers in the inlet to avoid the potential effect of ratchet number on the flow behavior. The resulting flow configuration is very similar to the longer ratchet inlet one though: the flow fluctuates between polarized and non-polarized states, exploring all the possible configurations.

C. Ratchet inlet and outlets

We then study the flow configurations of active nematics in bifurcation channels with ratchet inlets and outlets. The experimental results are shown in Fig.4. A general observation is that the peaks in the histograms are sharp, indicating that the flow configurations are more deterministic than in straight channels. When the outlet channels have different numbers of ratchet, as shown in Fig. 4(a) the flow robustly splits into different fractions in the two outlet channels. Interestingly, the flow rate ratio in the two outlet channels is almost equal to the ratio between the number of ratchet teeth. Does this unequal splitting of flow arise from the difference in the length of the channels? To answer this question, we keep the channels lengths unchanged, but modify the number of ratchet teeth in channel B, so that channels B and C has the same number of ratchet teeth. In this case, the flow robustly split into the two outlet channels with a 1:1 ratio, as shown in Fig.4(b). This result suggests that the ratchet teeth in the outlet channels play a dominant role in determining the flow behavior at bifurcations. In Fig.4(c), we show the flow behavior in channels with equal length and number of ratchet teeth. The flow again splits with a 1:1 ratio, confirming the dominant role of ratchet teeth.

[1] H Wioland, E Lushi, and R E Goldstein. Directed collective motion of bacteria under channel confinement. *New Journal of Physics*, 18(7):075002, July 2016. ISSN 1367-2630. doi:10.1088/1367-2630/18/7/075002.

- [2] Kun-Ta Wu, Jean Bernard Hishamunda, Daniel T. N. Chen, Stephen J. DeCamp, Ya-Wen Chang, Alberto Fernández-Nieves, Seth Fraden, and Zvonimir Dogic. Transition from turbulent to coherent flows in confined three-dimensional active fluids. *Science*, 355(6331):eaal1979, March 2017. ISSN 0036-8075, 1095-9203. doi: 10.1126/science.aal1979.
- [3] Alexandre Morin and Denis Bartolo. Flowing Active Liquids in a Pipe: Hysteretic Response of Polar Flocks to External Fields. *Physical Review X*, 8(2):021037, May 2018. doi:10.1103/PhysRevX.8.021037.
- [4] Jérôme Hardouin, Rian Hughes, Amin Doostmohammadi, Justine Laurent, Teresa Lopez-Leon, Julia M. Yeomans, Jordi Ignés-Mullol, and Francesc Sagués. Reconfigurable flows and defect landscape of confined active nematics. *Communications Physics*, 2(1):121, December 2019. ISSN 2399-3650. doi:10.1038/s42005-019-0221-x.
- [5] Jérôme Hardouin, Justine Laurent, Teresa Lopez-Leon, Jordi Ignés-Mullol, and Francesc Sagués. Active microfluidic transport in two-dimensional handlebodies. *Soft Matter*, 16(40):9230–9241, 2020. ISSN 1744-683X, 1744-6848. doi:10.1039/D0SM00610F.
- [6] Sumesh P. Thampi. Channel confined active nematics. *Current Opinion in Colloid & Interface Science*, 61:101613, October 2022. ISSN 1359-0294. doi:10.1016/j.cocis.2022.101613. URL <https://www.sciencedirect.com/science/article/pii/S1359029422000528>.
- [7] Francis G. Woodhouse and Jörn Dunkel. Active matter logic for autonomous microfluidics. *Nature Communications*, 8(1):15169, April 2017. ISSN 2041-1723. doi: 10.1038/ncomms15169.
- [8] Enkeleida Lushi, Hugo Wieland, and Raymond E. Goldstein. Fluid flows created by swimming bacteria drive self-organization in confined suspensions. *Proceedings of the National Academy of Sciences*, 111(27):9733–9738, July 2014. ISSN 0027-8424, 1091-6490. doi: 10.1073/pnas.1405698111.
- [9] Zhengyang Liu, Kechun Zhang, and Xiang Cheng. Rheology of bacterial suspensions under confinement. *Rheologica Acta*, 58(8):439–451, August 2019. ISSN 0035-4511, 1435-1528. doi:10.1007/s00397-019-01155-x.
- [10] Tyler D. Ross, Heun Jin Lee, Zijie Qu, Rachel A. Banks, Rob Phillips, and Matt Thomson. Controlling organization and forces in active matter through optically defined boundaries. *Nature*, 572(7768):224–229, August 2019. ISSN 0028-0836, 1476-4687. doi:10.1038/s41586-019-1447-1.
- [11] R Voituriez, J. F Joanny, and J Prost. Spontaneous flow transition in active polar gels. *Europhysics Letters (EPL)*, 70(3):404–410, May 2005. ISSN 0295-5075, 1286-4854. doi:10.1209/epl/i2004-10501-2.
- [12] Davide Marenduzzo. Hydrodynamics and Rheology of Active Liquid Crystals: A Numerical Investigation. 98: 118102, 2007. doi:10.1103/PhysRevLett.98.118102.
- [13] Tyler N. Shendruk, Amin Doostmohammadi, Kristian Thijssen, and Julia M. Yeomans. Dancing disclinations in confined active nematics. *Soft Matter*, 13(21):3853–3862, May 2017. ISSN 1744-6848. doi:10.1039/C6SM02310J.
- [14] Jaideep P. Vaidya, Tyler N. Shendruk, and Sumesh P. Thampi. Active nematics in corrugated channels. *Soft Matter*, September 2024. ISSN 1744-6848. doi: 10.1039/D4SM00760C. URL <https://pubs.rsc.org/en/content/articlelanding/2024/sm/d4sm00760c>. Publisher: The Royal Society of Chemistry.
- [15] Camille Jorge, Amélie Chardac, Alexis Poncet, and Denis Bartolo. Active hydraulics laws from frustration principles. *Nature Physics*, 20(2):303–309, February 2024. ISSN 1745-2481. doi:10.1038/s41567-023-02301-2. URL <https://www.nature.com/articles/s41567-023-02301-2>. Publisher: Nature Publishing Group.
- [16] S. Elizabeth Hulme, Willow R. DiLuzio, Sergey S. Shevkoplyas, Linda Turner, Michael Mayer, Howard C. Berg, and George M. Whitesides. Using ratchets and sorters to fractionate motile cells of Escherichia coli by length. *Lab on a Chip*, 8(11):1888, 2008. ISSN 1473-0197, 1473-0189. doi:10.1039/b809892a. URL <https://xlink.rsc.org/?DOI=b809892a>.
- [17] R. Di Leonardo, L. Angelani, D. Dell’Arciprete, G. Ruocco, V. Iebba, S. Schippa, M. P. Conte, F. Mecarini, F. De Angelis, and E. Di Fabrizio. Bacterial ratchet motors. *Proceedings of the National Academy of Sciences*, 107(21):9541–9545, May 2010. ISSN 0027-8424, 1091-6490. doi:10.1073/pnas.0910426107.
- [18] Sattvic Ray, Jie Zhang, and Zvonimir Dogic. Rectified Rotational Dynamics of Mobile Inclusions in Two-Dimensional Active Nematics. *Physical Review Letters*, 130(23):238301, June 2023. ISSN 0031-9007, 1079-7114. doi:10.1103/PhysRevLett.130.238301. URL <https://link.aps.org/doi/10.1103/PhysRevLett.130.238301>.
- [19] Tim Sanchez, Daniel T. N. Chen, Stephen J. DeCamp, Michael Heymann, and Zvonimir Dogic. Spontaneous motion in hierarchically assembled active matter. *Nature*, 491(7424):431–434, November 2012. ISSN 0028-0836, 1476-4687. doi:10.1038/nature11591.

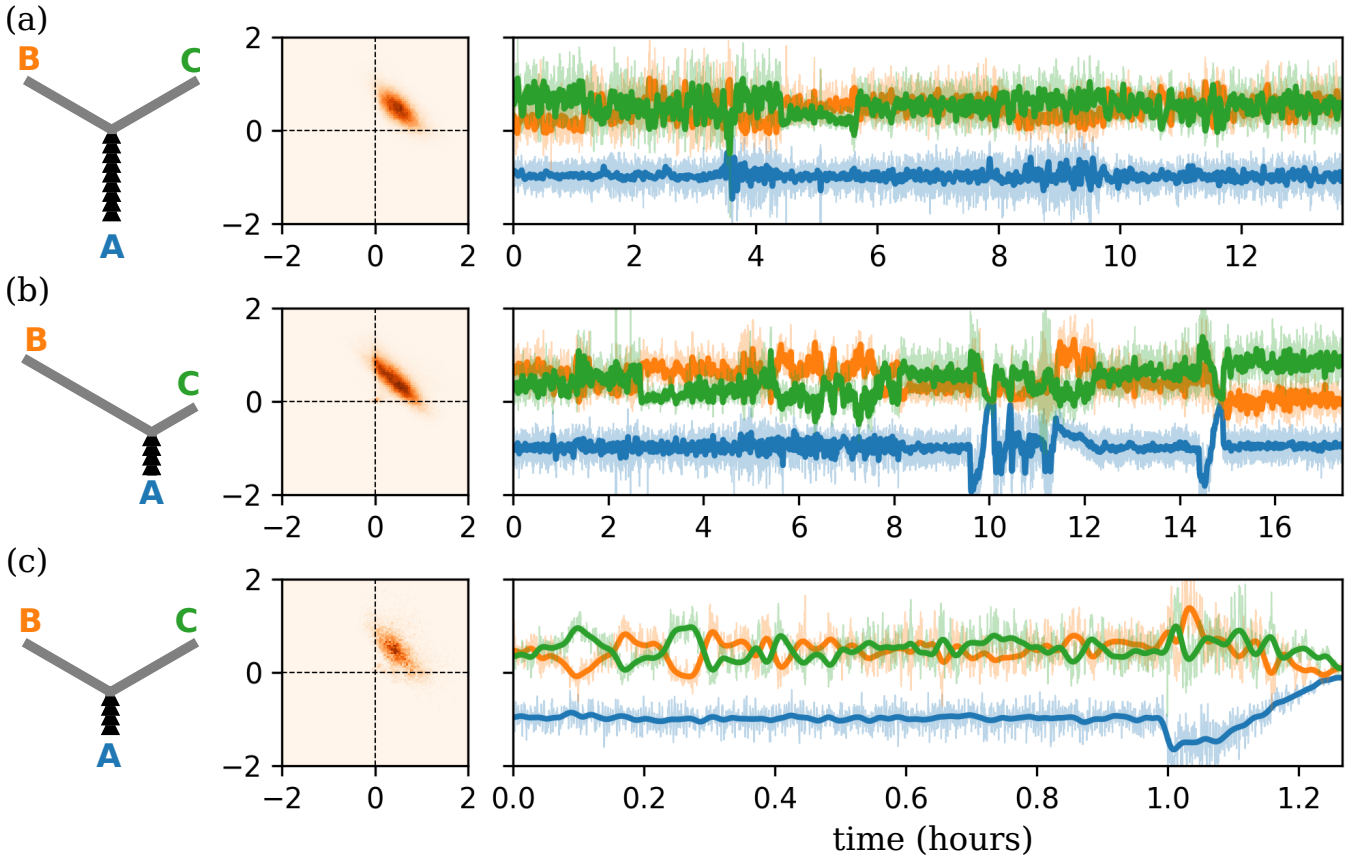


FIG. 3. Ratchet inlet and straight outlets: histogram and time series. (a) 9-teeth ratchet inlet with 2 equal length outlets. The flow fluctuates between polarized and non-polarized states, exploring all the possible configurations. The equal splitting state is the most probable configuration. (b) 4-teeth ratchet inlet with long and short outlets. The flow also explores all the possible configurations, but shows no preferred splitting ratio. (c) 4-teeth ratchet inlet with 2 equal length outlets. The flow fluctuates between polarized and non-polarized states, exploring all the possible configurations. The equal splitting state is the most probable configuration.

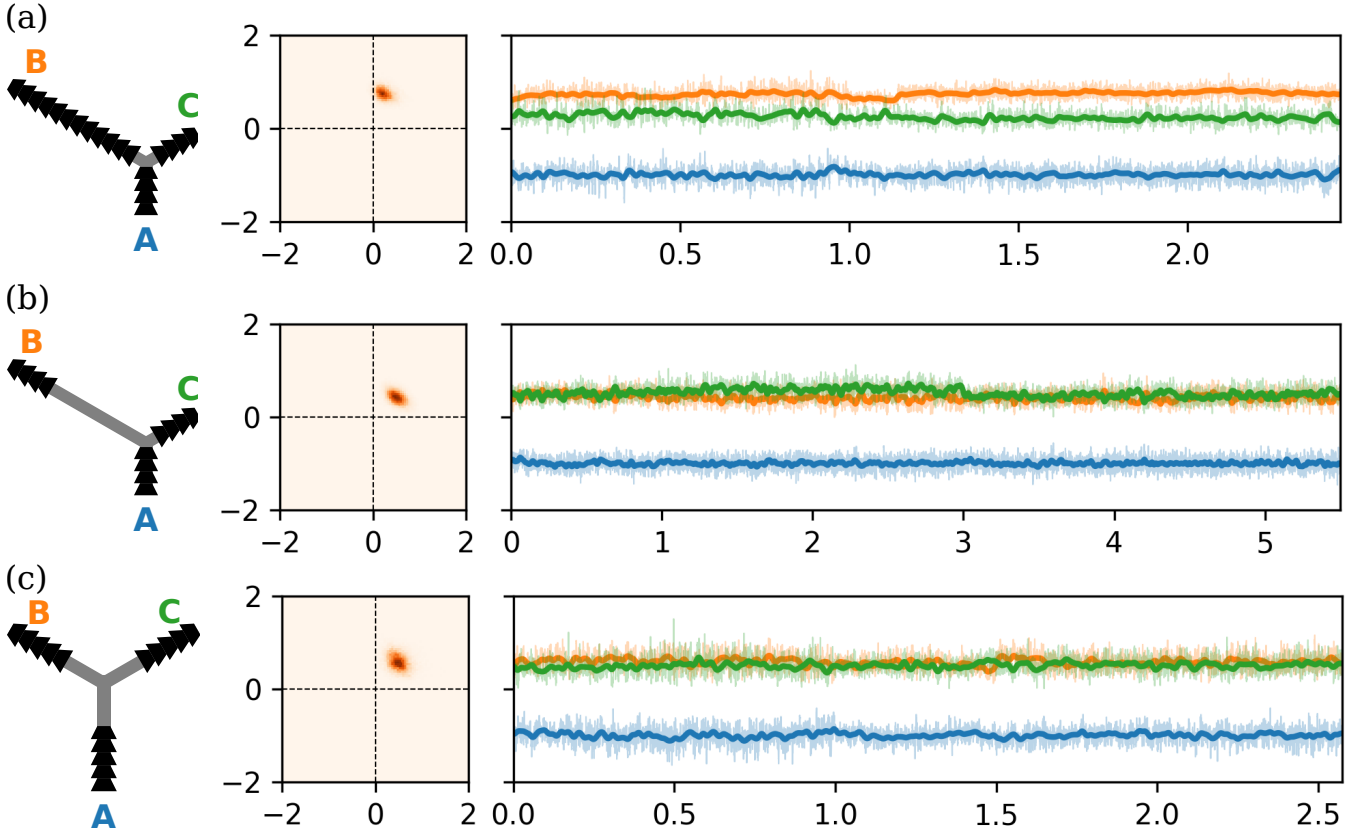


FIG. 4. Ratchet inlet and outlets: histogram and time series. (a) The numbers of ratchet teeth in channels A, B and C are 4, 13 and 4, respectively. Let's refer to this bifurcation channel network 4-13-4 bifurcation. In contrast to straight channels, the flows exhibit a sharp peak in the histogram, while other splitting ratios remain rarely explored. The splitting ratio is around 3:1. (b) 4-4-4 bifurcation, where channel B has an extended straight portion. The flows again exhibit a sharp peak in the histogram at a splitting ratio around 1:1. (c) 5-5-5 bifurcation, where all the channels are of the same length. The flows again exhibit a sharp peak in the histogram at a splitting ratio around 1:1.

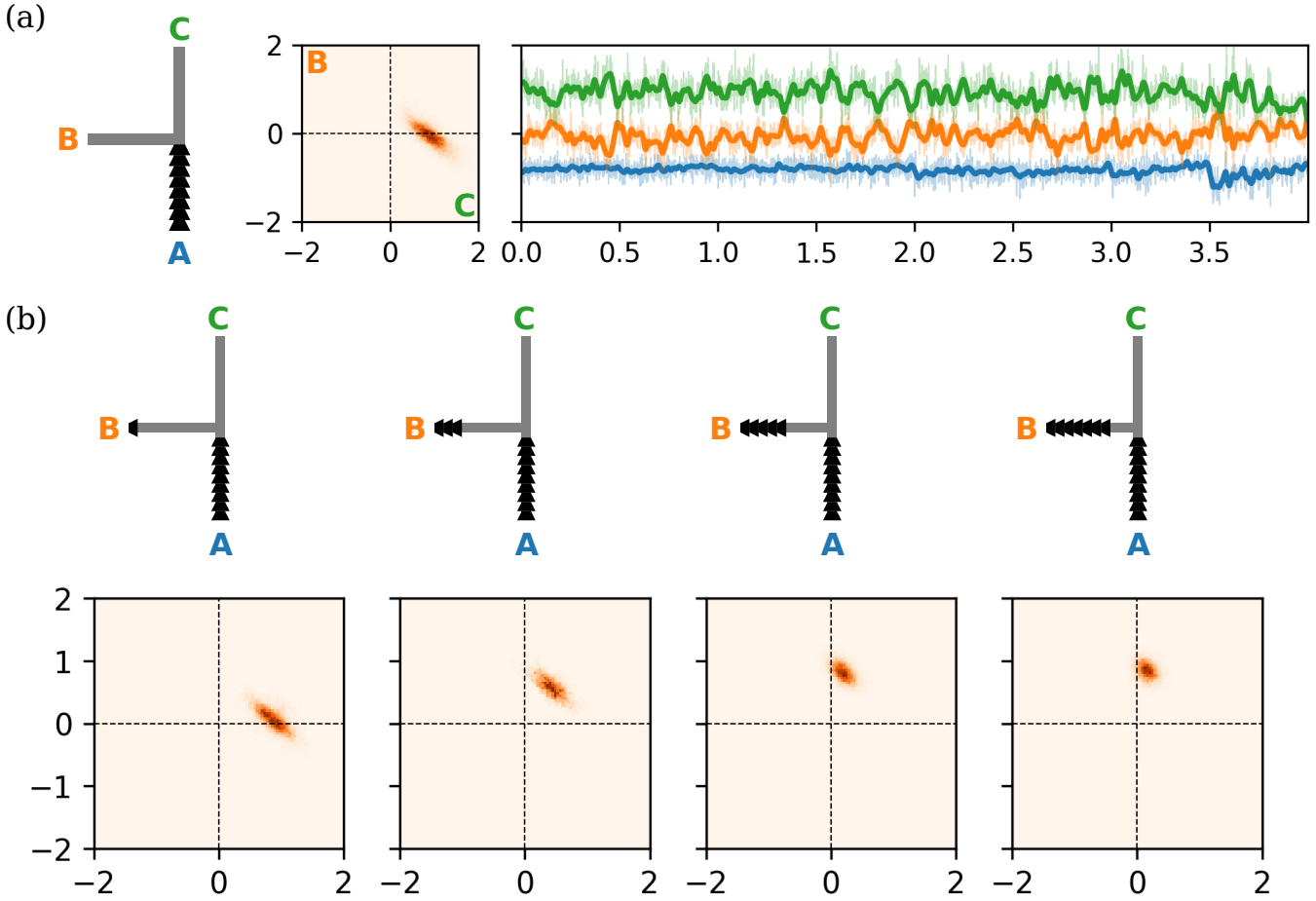


FIG. 5. **The role of turning angles.** (a) A bifurcation with a 9-teeth ratchet inlet and 2 straight outlets of the same length. The outlets have different turning angles with respect to the inlet channel A: $\angle AOB = 90^\circ$ and $\angle AOC = 180^\circ$. The flow rate histogram and time series suggest that the flow prefers the 180° channel C, i.e. the channel parallel to the inlet channel A, rather than channel B which requires a 90° turn. (b) Adding various numbers of ratchets to channel B to compete with the 90° turning angle. From left to right, 1, 3, 5, 7 ratchet teeth are added to the end of channel B. Below the schematics of bifurcation channels are the $\phi_B - \phi_C$ flow rate histograms corresponding to the design above. As the number of ratchet teeth in channel B is increased, the splitting ratio between B and C is increase from 0 to ∞ .